The Astronomical Journal, 157:22 (16pp), 2019 January https://doi.org/10.3847/1538-3881/aaf1ac
© 2018. The American Astronomical Society. All rights reserved.

Luminous and Variable Stars in NGC 2403 and M81*

Roberta M. Humphreys, Sarah Stangl, Michael S. Gordon, Kris Davidson, and Skyler H. Grammer
Minnesota Institute for Astrophysics, 116 Church Street SE, University of Minnesota, Minneapolis, MN 55455, USA; roberta@umn.edu
Received 2018 October 16; revised 2018 November 9; accepted 2018 November 14; published 2018 December 27

Abstract

We present the results of spectroscopy and multi-wavelength photometry of luminous and variable star candidates in the nearby spiral galaxies NGC 2403 and M81. We discuss specific classes of stars, the Luminous Blue Variables (LBVs), B[e] supergiants (sgB[e]), and the high-luminosity yellow hypergiants. We identify two new LBV candidates, and three sgB[e] stars in M81. We also find that some stars that were previously considered LBV candidates are actually field stars. The confirmed and candidate LBVs and sgB[e] stars together with the other confirmed members are shown on the HR Diagrams for their respective galaxies. We also present the HR Diagrams for the two "SN impostors", V37 (SN2002kg) and V12(SN1954J) in NGC 2403 and the stars in their immediate environments.

Key words: galaxies: individual (NGC 2403,M81) – supergiants

Supporting material: machine-readable table

1. Introduction

This paper is part of a series on the luminous and variable star populations in nearby resolved galaxies: the giant spiral M101 (Grammer et al. 2015) and the Local Group spirals M31 and M33, see Humphreys et al. (2017a) and other papers in the series. The primary goal of this work is a more comprehensive picture of the massive stars that define the upper HR Diagram with special emphasis on an improved census of those that experience high mass-loss episodes such as the Luminous Blue Variables (LBVs; Humphreys et al. 2016) and the evolved warm hypergiants (Humphreys et al. 2013; Gordon et al. 2016). In this paper, we present spectroscopy of luminous star candidates in the spiral galaxies NGC 2403 and M81.

Previous surveys of the stellar populations in these two galaxies began with the classic Tammann & Sandage (1968) study of NGC 2403. As part of his survey of the brightest stars in nearby galaxies, Sandage (1984a, 1984b) later presented color–magnitude diagrams for the candidate luminous stars in NGC 2403 and M81 based on photometry estimated from photographic plates. The first photographic spectra of a few of these stars in NGC 2403 and M81, previously identified by Sandage but not published, were described by Humphreys (1980). Digital spectra and near-infrared photometry for the red supergiant candidates (Humphreys et al. 1986) demonstrated that many of them were foreground dwarfs. Several of the blue star candidates were actually H II regions, especially in M81 (Humphreys & Aaronson 1987b). Zickgraf & Humphreys (1991) later produced catalogs of multi-color photometry of individual stars in NGC 2403 and M81 based on digitized scans of photographic plates. To accurately determine these stars' luminosities and place them on an HR Diagram requires confirming spectroscopy. Zickgraf et al. (1996) obtained moderate resolution spectra of the seven visually brightest blue supergiant candidates in M81, but concluded that most were compact H II regions or foreground dwarfs with one possible cluster member. Subsequently, Sholukhova et al. (1998b, 1998a) obtained spectra and identified several emission-line objects including LBV candidates in NGC 2403 and M81. Most recently, Kudritzki et al. (2012) reported the first quantitative analysis including metallicities, effective temperatures, and luminosities for 25 early-type supergiants in M81.

In this paper, we present additional blue and red spectra and multi-epoch imaging and photometry for the luminous star candidates in NGC 2403 and M81. In the next section, we describe our target selection, observations, and data reduction. In Section 3, we discuss specific stars such as LBVs and other emission-line stars. Multi-wavelength photometry and the spectral energy distributions (SEDs) are presented in Section 4 for stars that are candidates for high mass loss. We combine our results with previously published work and present the HR Diagrams for the confirmed members in NGC 2403 and M81 in the last section.

2. Data and Observations

2.1. Target Selection

Most of our targets were selected from the Zickgraf & Humphreys (1991) catalogs for NGC 2403 and M81 based on their apparent magnitude and color. We emphasized those most likely to be luminous early-type stars and suspected variables. To select additional candidates, we used aperture photometry measured from the Hubble Legacy Archive (HLA) Advanced Camera for Survey (ACS) images of NGC 2403 and M81 in the ANGRRR and ANGST programs.[1] Known variables from Tammann & Sandage (1968) and several stars with previously observed spectra (Humphreys & Aaronson 1987b; Zickgraf et al. 1996; Sholukhova et al. 1998b, 1998a) were also included. For the fiber assignment with the MMT/Hectospec,

* Based on observations with the Multiple Mirror Telescope, a joint facility of the Smithsonian Institution and the University of Arizona and on observations obtained with the Large Binocular Telescope (LBT), an international collaboration among institutions in the United States, Italy and Germany. LBT Corporation partners are: The University of Arizona on behalf of the Arizona university system; Istituto Nazionale di Astrofisica, Italy; LBT Beteiligungsgesellschaft, Germany, representing the Max-Planck Society, the Astrophysical Institute Potsdam, and Heidelberg University; The Ohio State University, and The Research Corporation, on behalf of The University of Notre Dame, University of Minnesota and University of Virginia.

[1] Proposals GO-10182, GO-10579, and GO-10584.

Table 1
Journal of Observations

Target	Date (UT)	Exp. Time (minutes)	Grating, Tilt	Comment
NGC2403-F1 Red	2012 Oct 10	180	600l, 7200 Å	…
NGC2403-F2 Red	2012 Nov 4	150	600l, 7200 Å	…
NGC2403-F1 Blue	2012 Dec 4	120	600l, 4800 Å	…
NGC2403-F2 Blue	2012 Dec 4	225	600l, 4800 Å	…
NGC2403-F1 Blue	2012 Dec 5	120	600l, 4800 Å	…
NGC2403-F2 Blue	2012 Dec 5	30	600l, 4800 Å	…
M81 Blue	2012 Feb 22	150	600l, 4800 Å	partly cloudy
M81 Red	2012 Feb 22	90	600l, 7200 Å	partly cloudy
M81 Blue	2012 Mar 15	120	600l, 4800 Å	…
M81 Blue	2014 Feb 20	135	600l, 4800 Å	clouds, high Z, not used
M81 Blue	2014 Feb 21	135	600l, 4800 Å	…
M81 Red	2014 Feb 28	180	600l, 7200 Å	…

Note. "F1" was centered at 07:36:25.89+65:38:48.4 and "F2" was centered at 07:36:23.19+65:34:54.2.

targets were ranked based on their apparent magnitudes, colors, previous spectra suggesting that they may be supergiants, and on their variability. Since one of our goals is to identify stars that may be candidates for high mass loss, we used the LBT nearby galaxy survey (Kochanek et al. 2008; Gerke et al. 2014) to initially identify candidates for variability as described in Grammer et al. (2015). We identified targets as potentially variable if their rms variability is greater than their median photometric error. The brightest stars, based on their apparent V magnitude with clear indications of variability, received the highest priority, rank 1, for spectroscopy with the Hectospec. The light curves for several of these stars are shown and discussed in Section 3.

Following these criteria, we selected 124 stars in NGC 2403 with V magnitudes between 18.0 and 20.1, and 91 in M81 with V magnitudes between 18.5 and 20.1. Eighty-six in NGC 2403 were assigned fibers in two separate pointings, fields F1 and F2, and 61 stars in M81 were assigned fibers.

2.2. Spectroscopy

The spectra were observed with the Hectospec, a multi-object spectrometer mounted on the MMT (Fabricant et al. 1998, 2005). The Hectospec[2] is a fiber-fed MOS with a 1° FOV and 300 fibers; each fiber subtends 1$''$.5 on the sky. We used the 600 mm^{-1} grating with the blue tilt centered on 4800 Å and the red tilt centered on 7300 Å. The red tilt was chosen to include Hα plus the Ca II triplet at ∼8500 Å. The 600 mm^{-1} grating gives a spectral coverage of ∼2500 Å with 0.54 Å pixel^{-1} resolution. The journal of observations is given in Table 1.

The NGC 2403 targets were observed in 2012 October and December in two fields, F1 and F2. The total exposures times in the blue were 4H and 4H 15M for F1 and F2, respectively, and for the red spectra, 3H for F1 and 2.5H for F2. The two pointings overlapped so that 27 stars were in common yielding total integration times of 8.25H in the blue and 5.5H in the red for these stars. Unfortunately, the M81 observations were plagued by poor observing conditions. Consequently, the spectra were acquired over two observing seasons in 2012 and again in 2014. The three best sets of blue spectra were combined to give a total integration time of 6.75H. Since two of the data sets were separated in time, the spectra provide an opportunity to check for spectroscopic variability before being combined. The red spectra were likewise observed in the two seasons for a total integration time of 4.5H.

The spectra were reduced using an exported version of the CfA/SAO SPECROAD package for Hectospec data E-SPECROAD.[3] The spectra were bias subtracted, flat-fielded, wavelength calibrated, and sky subtracted. The reduced spectra are available at http://etacar.umn.edu/LuminousStars/NGC2403M81/.

3. Classification of the Stars in NGC 2403 and M81

Spectral classification of the confirmed members are given in Tables 2 and 3 for NGC 2403 and M81. The tables also include positions, visual magnitudes, the target source, and comments on the spectrum and observations. Nonmembers or foreground stars plus some likely background QSOs are listed in Table 7 in Appendix A. We also include snap-shot images when available, Figures 12 and 13 in Appendix B.

In the following subsections, we describe specific stars of interest with examples of their spectra and light curves for the variables.

3.1. Emission-line Stars, Hot Supergiants, and WR Stars

Although our selection criteria favored the visually brightest stars of spectral types A and F, we identified 10 hot or emission-line stars in NGC 2403 and six in M81. Three B[e] supergiant candidates in M81 and two WN stars in N2403 are described here.

The B[e] supergiants share many spectral characteristics with LBVs (Humphreys et al. 2017c) including prominent Fe II and [Fe II] emission. In a recent spectroscopic survey of emission-line stars, Aret et al. (2016) designated [O I] $\lambda\lambda$6300,6364 emission as one of the characteristics of the sgB[e] class. [O I] emission is not observed in confirmed LBVs and can be used to separate the two types (Humphreys et al. 2017c). But these lines are also present in the night sky spectrum and in H II regions. For faint stars in N2403 and M81, this can be a problem, with contaminating nebulosity in the aperture and

[2] http://www.cfa.harvard.edu/mmti/hectospec.html

[3] External SPECROAD was developed by Juan Cabanela for use on Linux or MacOS X systems outside of CfA. It is available online at http://iparrizar.mnstate.edu.

Table 2
Members of NGC 2403

Star ID	Position*J*2000	Sp. Type	*V*	Source[a]	Variability	Comments
ZH 585 (F1+F2)	7:35:37.75 65:35:33.77	F2 I	19.43	1	⋯	Hα em, neb em
ZH 553 (F1+F2)	7:36:10.10 65:33:30.91	A8 I	⋯	1	no	see the text
ZH 335 (F1+F2)	7:36:12.02 65:32:44.39	F0 I	19.19	1	no	neb em
ZH 2387 (F1+F2)	7:36:15.63 65:40:43.15	H II	20.2	1	⋯	He I em
ZH 2352 (F1)	7:36:16.59 65:37:34.58	H II	19.65	1	⋯	
ZH 1593 (F2)	7:36:16.79 65:37:25.45	H II	19.28	1	⋯	strong neb em, He I em
ZH 755 (F1+F2)	7:36:19.67 65:39:3.09	H II	20.15	1	⋯	He I, N II λ5670 em
ZH 2341 (F1)	7:36:20.06 65:37:29.73	H II	18.42	1	⋯	He I em
ZH 2072 (F1)	7:36:23.69 65:36:19.58	H II	20.13	1	⋯	He I em
ZH 2331 (F2)	7:36:24.55 65:37:57.83	H II	19.94	1	⋯	strong neb em, He I em
ZH 2328 (F1)	7:36:25.14 65:37:57.90	hot star	20.04	1	⋯	neb em, He I em, Hα broad wings
ZH 1521 (F1)(10579-x1-7)	7:36:25.92 65:35:31.23	F2 I	18.59	1	⋯	neb em
ZH 2306 (F2)	7:36:37.50 65:37:54.47	H II	18.28	1	⋯	strong neb em, He I em
ZH 533 (F1+F2)	7:36:37.57 65:33:33.47	B5: I	19.36	1	no	neb em, He I abs, λ7774 abs
ZH 2313 (F1)	7:36:39.21 65:39:33.89	A0-A2	19.78	1	⋯	neb em, Hα wings
ZH 2562 (F1)	7:36:44.36 65:39:11.25	B I	19.57	1	⋯	neb em, He I abs, N II λ 5670 em
ZH 2022 (F1)	7:36:44.73 65:33:25.87	B8 I	19.95	1	⋯	neb em, Hβ P Cyg + wings, Hα broad wings
10182-pr-9 (F2)	7:36:45.49 65:37:0.83	WN:	⋯	2	⋯	[N II] em, H, He I em, Hα wings
ZH 2016 (F2)	7:36:47.84 65:33:26.08	WN:	18.47	1	⋯	strong neb em, N II, He I em
10579-x1-3 (F1)	7:36:48.56 65:36:45.50	neb em	20.3	3	⋯	H em. superposed on abs.
10182-pr-1 (F1)	7:36:48.79 65:35:52.74	A5-A8 I	⋯	2	⋯	strong neb em
ZH 946 (F2)	7:36:50.63 65:38:49.10	B5 I:	19.74	1	⋯	neb em, Horiz Br?
ZH 947 (F1)	7:36:51.44 65:39:0.47	B5 I	19.06	1	⋯	neb em, He I abs
10182-pr-2 (F1)	7:36:56.20 65:36:42.04	F5 I	18.83	2	var	neb em, Hα P Cyg
ZH 2554 (F1+F2)	7:36:58.28 65:41:5.59	H II	20.2	1	⋯	He I em
10182-pr-6 (F1)	7:36:59.12 65:35:9.95	A8-F0 I	18.79	2	⋯	strong neb em, He I λ6678,7065 P Cyg, Ca II abs, probable blend
10182-pr-15 (F2)	7:36:59.12 65:35:17.97	A0-A2 I	19.52	2	⋯	strong neb em, He I abs, Mg II abs
10182-pr-16 (F2)	7:37:01.34 65:34:26.06	B8 I:	19.35	2	⋯	He I abs
ZH-729 (F2)	7:37:01.62 65:37:31.95	B8 I	19.21	1	⋯	neb em, H em in abs core, He I abs
V37 (F1)	7:37:01.83 65:34:29.3	LBV	20.6	4	var	see Humphreys et al. (2017b)
ZH 2248 (F2)(10402-7)	7:37:6.56 65:33:54.21	A0 I	19.71	1	var	neb em
V38 (F1)	7:37:10.6 65:33:10	LBV	19.4	4	var	neb em, see the text
ZH 931 (F1)	7:37:10.77 65:39:41.59	A5-A8 I	19.95	1	⋯	Hα core em
ZH 1938 (F1)	7:37:12.02 65:32:1.15	A2 I	19.36	1	var	neb em
S94 (F1)	7:37:12.79 65:36:12.68	F5 I	18.78	5	var:	see the text
ZH 924 (F1)	7:37:15.47 65:38:38.04	B5-B8 I	19.3	1	⋯	neb em, He I abs
ZH 1483 (F2)	7:37:15.76 65:32:02.11	H II	18.54	1	⋯	strong neb em, He I em
ZH 2212 (F2)	7:37:21.07 65:33:5.86	H II	19.9	1	⋯	neb em, He I em
ZH 912 (F1)	7:37:32.86 65:38:59.49	A0-2 I	18.41	1	⋯	neb em, He I λ6678 abs, λ7774 abs, A8 Ia(Humphreys & Aaronson 1987b)
ZH 884 (F1+F2)	7:37:48.92 65:35:37.79	F0 I	18.78	1	⋯	neb em, double Hα

Note.
[a] Primary Sources for targets: (1) Zickgraf & Humphreys (1991), (2) GO-10182, (3) GO-10579), (4) Tammann & Sandage (1968), (5) Sandage (1984a).

residual or poor sky subtraction. For that reason, we rely on the velocity of the [O I] lines to identify them with the star, i.e., if they have the same velocity as the He I and the Fe II lines presumably formed in the circumstellar ejecta, although they may be nebular in origin.

With this criterion, we identified three possible sgB[e] stars in M81: 10584-4.1, 10584-8.4, and 10584-9.1. Their blue and red spectra are shown in Figure 1. All three stars have prominent Balmer emission with P Cyg profiles and Fe II and Fe[II] lines in the blue plus the λ6300,6363 [O I] lines in the red. He I is also in emission with P Cyg profiles in all three stars. Thus, they all show evidence for stellar winds and mass loss. Their outflow velocities, measured from the absorption minima in their P Cygni profiles relative to the emission-line peak indicate moderate wind speeds of 170–180 km s^{-1} for 10584-8.4 and 10584-9.1 and 250 km s^{-1} for 10584-4.1. These velocities, measured in the same way, are typical of other sgB[e] stars as well as LBVs (Humphreys et al. 2016). We note that 10584-4.1 and 10584-9.1 are spectroscopically very similar. Both also have broad Thomson scattering wings on their Hα and Hβ emission profiles.

The spectrum of 10584-8.4 shows several absorption lines including some He I lines, which, together with other lines such as Mg II, λ4481, permit us to estimate a late B/early A spectral type for this star. 10584-8.4 also has the [Ca II] doublet at λλ7291,7324 in emission, another characteristic of some of the sgB[e] stars, shared with the warm hypergiants (Humphreys et al. 2017c). The Ca II triplet line near λ8500 can also be seen

Table 3
Members of M81

Star ID	Position J2000	Sp. Type	V	Source[a]	Variability	Comments
ZH 501	9:54:34.86 69:05:53.72	H II	18.19	1	…	strong neb em, He I em
10584-11-3	9:54:41.4514 69:04:08.81	H II	20.08	2	…	strong neb em, He II em, hot star blend?
10584-11-1	9:54:42.48 69:2:57.04	A5 I	19.38	2	var	H em
10584-11-2	9:54:42.57 69:03:38.08	H II	19.81	2	…	strong neb em, He I em
ZH 679	9:54:45.40 69:9:26.42	A8 I	19.7	1	…	H em
10584-8-4	9:54:50.03 69:6:55.47	sgB[e]	…	2	…	H em P Cyg,He I, Fe II, [Ca II] em, see the text
10584-4-1	9:54:54.05 69:10:23.00	sgB[e]	19.68	2	var	H em, P Cyg, He I, Fe II em, see the text
ZH 372(10584-15-1)	9:54:56.92 69:01:3.67	F5 I	19.64	1, 2	…	
ZH 1434	9:55:00.79 69:13:4.32	H II	20.12	1	…	strong neb em, He I em
10584-8-1	9:55:01.39 69:07:06.02	F0 I	19.16	2	var:	
10584-8-2	9:55:09.01 69:07:08.27	F0 I	19.46	2	…	H em
ZH 244(I1)(10584-19-1)	9:55:12.78 68:59:45.74	A I	20.35	1, 2, 3	var	low S/N, Hα em
10584-9-1	9:55:18.97 69:08:27.54	sgB[e]	19.1	2	var	H em P Cyg, He I, Fe II em, see the text
ZH 364(I2)(10584-16-1)	9:55:20.31 69:01:55.97	LBVc[b]	19.59	1, 2, 3	var	H, He I, Fe II, N II em, Hα wings, see the text
ZH 235	9:55:22.52 68:58:32.85	H II	20.26	1	…	strong neb em, He I em
10584-5-2	9:55:25.61 69:12:14.00	F5 I	19.98	2	…	neb em
ZH 224 (10584-23-1)	9:55:34.51 68:55:48.50	F 2-5 I	18.83	1, 2	var:	strong neb em
10584-13-2	9:55:40.25 69:7:31.24	F2 I	19.8	2	…	H em
10584-10-5	9:55:41.24 69:11:02.53	A I + WN	19.65	2	…	blend, [N II] em + neb em
10584-20-2	9:55:53.35 68:59:04.49	B5 I	17.49	2	…	strong neb em, He I em, P cyg
10584-13-3	9:55:58.33 69:06:44.95	F8 I	19.62	2	var:	
ZH 354	9:56:01.36 68:59:49.37	LBVc (Of/ late WN:)	19.6	1	var:	H, strong N II, He II λ4686 em, see the text
10584-14-2	9:56:09.02 69:05:55.49	G0 I	19.65	2	…	
ZH 1143 (10584-24-1)	9:56:9.12 68:56:43.78	F2 I	18.76	1	…	H em, neb em, M81-75
ZH 1406(I8)(10584-18-1)	9:56:14.76 69:05:19.88	F5 I	19.26	1, 2, 3	var:	neb em
10584-25-2	9:56:15.70 68:58:32.63	G0 I	19.24	2	var	neb em
ZH 348	9:56:24.51 68:59:15.91	H II	18.94	1	…	neb em, He I em
10584-18-5	9:56:32.36 69:05:08.99	A8 I	19.74	2	…	

Notes.
[a] Primary Sources for targets: (1) Zickgraf & Humphreys (1991), (2) GO-10584, (3) Sandage (1984a).
[b] Candidate LBV.

in emission at the red edge of the spectrum. It shows a split profile, which could be due to a bipolar outflow or rotation, a characteristic also observed in some sgB[e]'s. The peaks are separated by 108 km s^{-1}. 10584-4.1 and 10584-9.1 are apparently much warmer stars. There are no obvious absorption lines in either spectrum. In addition to strong He I, the OI lines at λ7774 and λ8446 are also in emission in 10584-4.1.

Light curves for 10584-4.1 and 10584-9.1 are shown in Figure 2, but there is insufficient data for 10584-8.4. 10584-4.1 shows significant variability over five years by 0.2 to 0.4 mag in the U, V, and R bands. 10584-9.1 declined by about 0.5 mag from 2011 to 2013. Thus, both stars are variable.

We also identify two late WN stars in N2403: 10182-pr-9 and ZH 2016. The blue spectra of both show prominent broad nitrogen emission features from 4630 to 4700 Å and from 5670 to 5700 Å with strong H and He I emission lines. He II λ 4686 emission is present in 10182-pr-9.

3.2. Intermediate-Type Supergiants

The A- and F-type supergiants are the visually brightest stars. They define the upper luminosity boundary in the HR diagram for evolved post-main-sequence massive stars with initial masses typically less than 40–50 $M_{\odot}$ (Humphreys & Davidson 1979, 1994). Many stars that lie near this boundary show evidence for high and episodic mass loss in their spectra and spectral energy distributions (Humphreys et al. 2013). Blue and red spectra of two luminous intermediate-type supergiants are shown in Figure 3.

ZH 553 in N2403 is a late A-type supergiant of high luminosity. It is known as star IVa28 in previous publications (Humphreys & Aaronson 1987a, 1987b). Its red spectrum shows Hα plus the [N II] and [S II] nebular lines in emission. The Hα profile is asymmetric to the red with broad wings characteristic of Thomson scattering in its wind plus P Cygni absorption. The star is thus experiencing mass loss with a moderately slow outflow velocity of 98 km s^{-1} measured from the P Cyg absorption minimum relative to the emission peak. The nebular lines appear to be double peaked. We noticed this in several stars in our similar survey of stars in M101 (Grammer et al. 2015), which in M101 we suspected may be due to emission from two sides of large H II regions or from more than one emission region along the line of sight. Since ZH 553 does not have strong [O III] nebular emission lines in the blue, the double peaks may rise either from contaminating emission in the aperture plus nebular emission from its circumstellar ejecta, or from the two sides of its expanding ejecta. The velocity difference between the blue and red

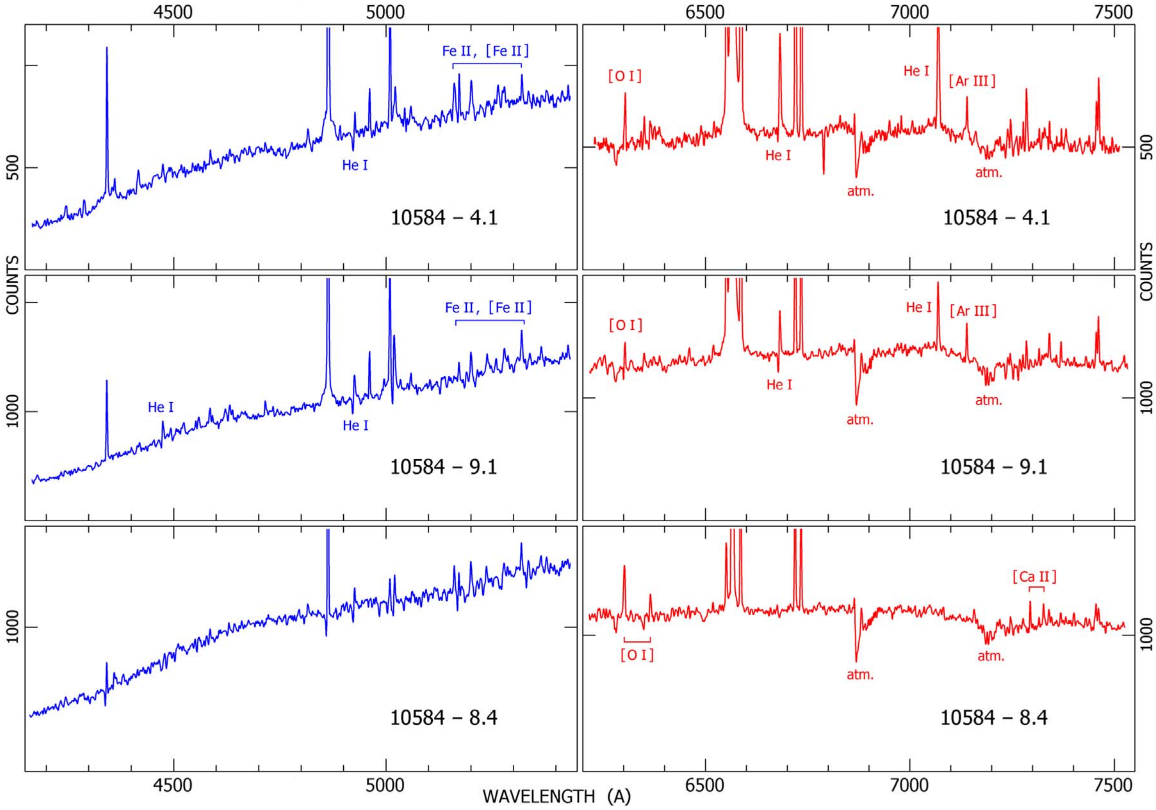

Figure 1. Blue and red spectra of three B[e] supergiants in M81.

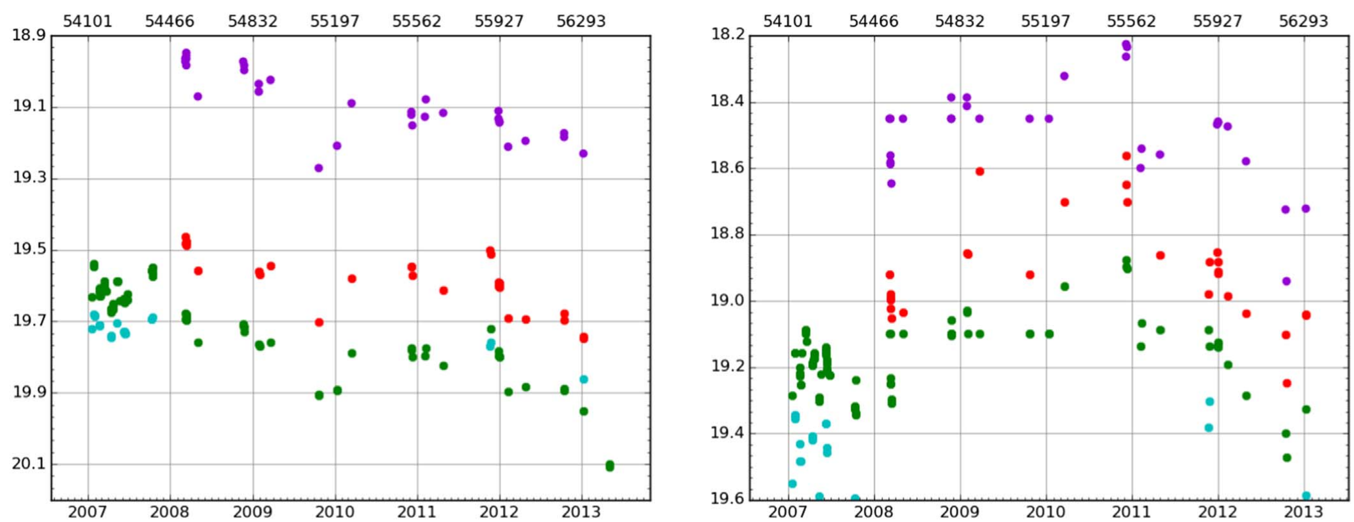

Figure 2. Multi-color light curves for the B[e] supergiants 10584-4.1 and 10584-9.1. The *U* band measurements are shown in violet, *B* band in blue, *V* in green, and *R* in red. The formal errors in the LBT/LBC photometry are smaller than the dots.

components average $56\ \mathrm{km\ s^{-1}}$. There are no other emission lines in the blue or red spectra.

S94 was originally listed by Sandage (1984a) as one of the brightest resolved objects in N2403. It has the spectrum of a high-luminosity F-type supergiant. The red spectrum shows Hα plus the [N II] and S[II] nebular lines in emission, and [O III] λ5007 is visible in emission in the blue spectrum. Hα has a P Cygni absorption feature. The absorption minimum relative to the peak emission has an expansion velocity of $143\ \mathrm{km\ s^{-1}}$ indicating a slow wind and mass loss typical of luminous intermediate-type supergiants.

Both ZH 553 and S94 have marginal variability of 0.1 mag or less. Their Balmer emission lines with P Cyg profiles and evidence for mass loss are typical of luminous intermediate-type supergiants, but neither show evidence for circumstellar dust (Section 4.1). We do not consider either to be an LBV/S Dor candidate.

3.3. Luminous Blue Variables and Candidates

The Tammann & Sandage (1968) survey identified several irregular blue variables in N2403. The most famous is V12,

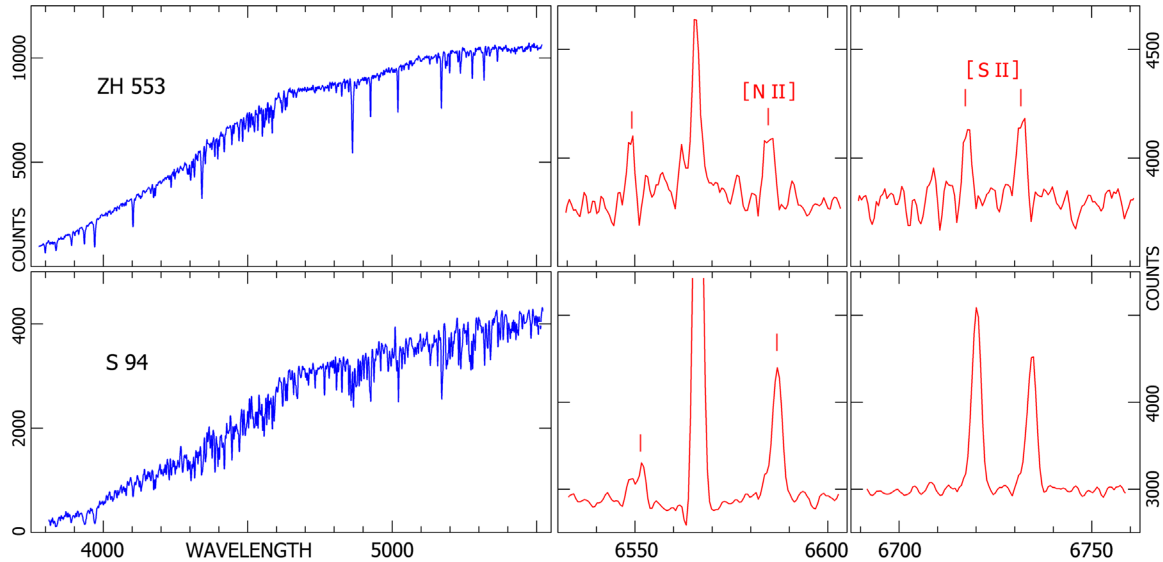

Figure 3. Blue and red spectra of two intermediate-type supergiants ZH 553 (A8 Ia) and S94 (F5 Ia). Note the double peaked nebular emission lines in ZH 553, and a probable P Cygni absorption feature in the broad asymmetric Hα emission profile. S94 also has a P Cygni absorption feature at Hα.

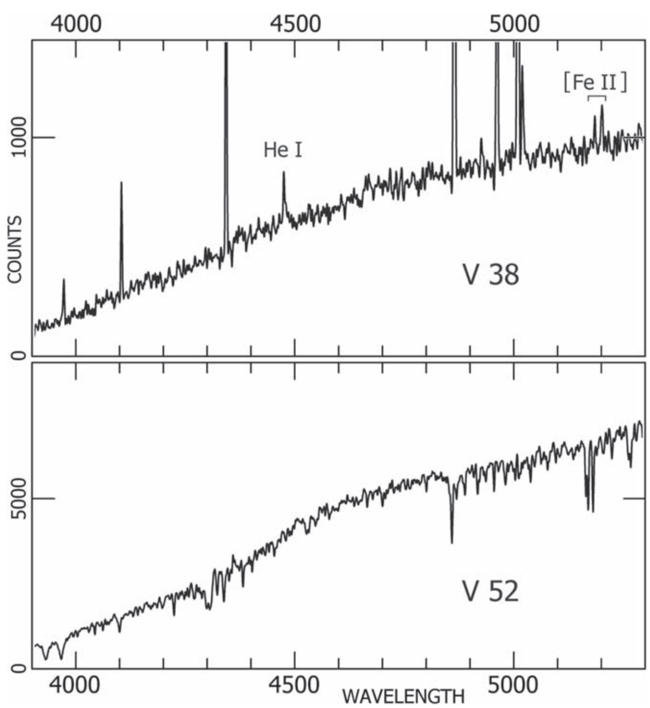

Figure 4. Blue spectra of V38 and V52 in N2403. V38 is an LBV while V52 is a foreground F-type dwarf.

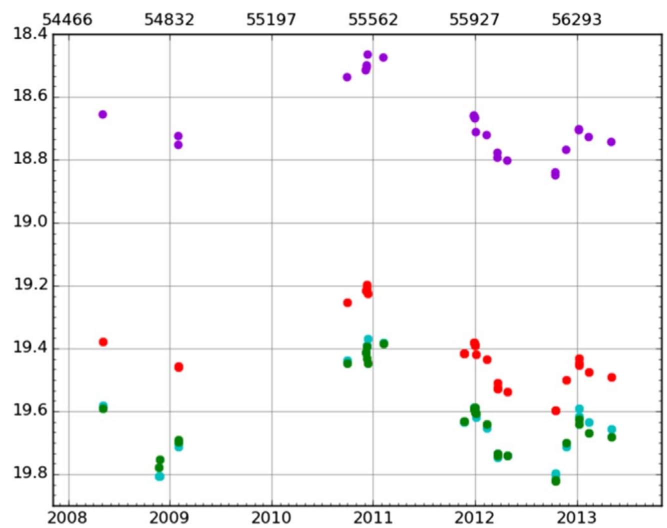

Figure 5. The multi-color light curve for N2403-V38. The color code is the same as in Figure 2.

also known as SN 1954J, which had a non-terminal giant eruption. Another, V37 also received a supernova designation as SN 2002 kg due to what was soon recognized as a typical LBV/S Dor high mass loss or maximum light event. In a recent paper on these two "impostors", we discussed the spectrum and light curve of V37 in some detail and showed that its progenitor was an evolved massive star of $\sim 60\, M_{\odot}$ (Humphreys et al. 2017b). V12 or SN 1954J survived its giant eruption and is now obscured by circumstellar dust from that eruption. Our spectral analysis revealed that V12 is actually two stars: a $\sim$20000 K star, which is the probable progenitor and survivor of the giant outburst, plus a G-type supergiant close neighbor or companion. Interestingly, we find that the hot star was initially only about $20\, M_{\odot}$ and the G supergiant of slightly lower mass. The HR Diagram for V12 and V37 and their stellar environments is discussed in Section 5.

Here we include spectra of two additional blue variables in N2403: V38 and V52. Based on the low-resolution spectrum of V38 shown in Humphreys & Aaronson (1987b), we suggested that it was an LBV or LBV candidate. Our higher-resolution blue and red spectra and their variability now confirm that designation. The blue spectrum (Figure 4) shows strong nebular and Balmer emission with He I and Fe II emission lines. N II absorption lines are present at λ5660–5680 Å. Hα has broad wings, and a P Cyg absorption feature is present at Hβ. The [O I] emission lines in the red spectrum at $\lambda\lambda$6300,6363 are also present, at the same velocities as the nebular lines. Thus, we suspect that they are nebular in origin,

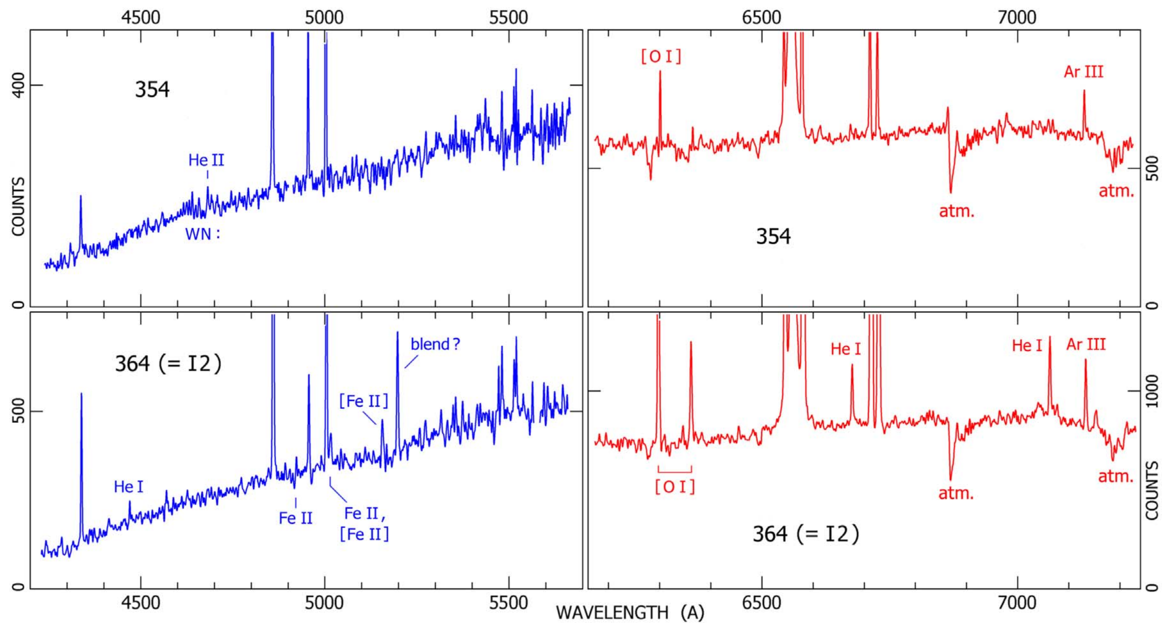

Figure 6. Blue and red spectra of two LBV candidates in M81: ZH 354 and I2 (ZH 364). A small gap at ∼4900 Å in ZH 354 is due to a flaw in the data.

and the star is not an sgB[e]. Its light curve in Figure 5 shows short-term variability of a few tenths of a magnitude.

V52, however, is a foreground late F-type dwarf (Figure 4). Its variability reported by Tammann & Sandage (1968) was marginal, and the LBT survey did not show any variability.

Sandage (1984b) identified six irregular blue variables in M81. We observed four of them: I1 (ZH 244), I2(ZH 364), I8(ZH 1406), and I3. I3 is a foreground F5 dwarf. I2 was observed in our earlier study (Humphreys & Aaronson 1987b), and based on its low-resolution spectrum, we considered it a candidate LBV(LBVc). Our new blue and red spectra (Figure 6) reveal a complex spectrum with emission lines of H, He I, and Fe II and [Fe II]. Strong nebular emission lines are also present. The nebular lines have a somewhat different average velocity of ≈ -130 km s^{-1} compared to the He I, H and Fe II emission with velocities of -80 to -100 km s^{-1}. The [O I] lines at 6300 Å have velocities of -125 km s^{-1}, so we assume that they are nebular in origin and are not from the star.

I8 is an F5 supergiant. Its blue spectrum does not show any emission lines. The red spectrum has strong nebular emission but no other emission lines. I8's variability is marginal. Thus, we do not consider it an LBV or candidate. It is worth noting that during their high mass loss or dense wind state, LBV/S Dor variables have absorption line spectra that resemble A or F-type supergiants due to their optically thick cool winds. Thus the "less luminous" LBV/S Dor variables (Humphreys et al. 2016), when in "eruption", overlap the position of the normal luminous intermediate temperature supergiants on the HR Diagram, but LBVs in "eruption" also have strong H emission with prominent P Cyg profiles and Fe II emission.

The blue spectrum of I1 has a low signal-to-noise ratio (S/N), limiting the accuracy of the classification, but its lines are consistent with a late B- or early A-type supergiant. The only emission line is Hα with wings that are asymmetric to red. I1 apparently has a stellar wind, but there are no P Cyg features or other emission lines. Its light curve (Figure 7) however shows a pattern of smooth variability over five years. It may be similar to M33C-4640 (Humphreys et al. 2016, 2017c), a candidate for post-RSG evolution.

ZH 354 in M81 is another emission-line star that we include here as a candidate LBV (Figure 6). The [O I] $\lambda\lambda$6300,6363 lines are present, but their near-zero velocities compared with -220 to -250 km s^{-1} velocities of the other emission lines confirm that they are residual night sky lines. ZH 354 also has features in common with the Of/WN stars. Its spectrum shows strong Balmer emission, nitrogen emission in the λ4600 to 4700 Å region with He II λ4686 in emission. There is no obvious He I emission in the rather low-S/N spectrum. Hα has very broad wings but with no P Cygni absorption. Its light curve shows only marginal variability of ± 0.1 mag over five years. Many LBVs in their quiescent state have Of/late WN features, so it is possible that ZH 354 is an LBV in quiescence.

The light curves of I2 (ZH 364), I1 (ZH 244) and ZH 354 are shown in Figure 7.

Based on our spectra and the available light curves, V37 and V38 in N2403 are confirmed LBV/S Dor variables, and I2(ZH 364) and ZH 354 in M81 should be considered candidate LBVs.

3.4. Comparison with other Surveys

In addition to our previous papers (Humphreys & Aaronson 1987a, 1987b), Sholukhova et al. (1998b, 1998a) observed several of the stars listed by Sandage (1984a, 1984b) plus others from Zickgraf & Humphreys (1991) and Zickgraf et al. (1996). Based on their classification of several as LBV candidates, we included them on our program but found that most are not LBVs. As already described above, S94 is a very luminous F-type supergiant but not an LBV candidate while V52 is a foreground dwarf. For convenience and ease of comparison, we list the stars in common with previous work in Table 4, together with our classifications in this paper.

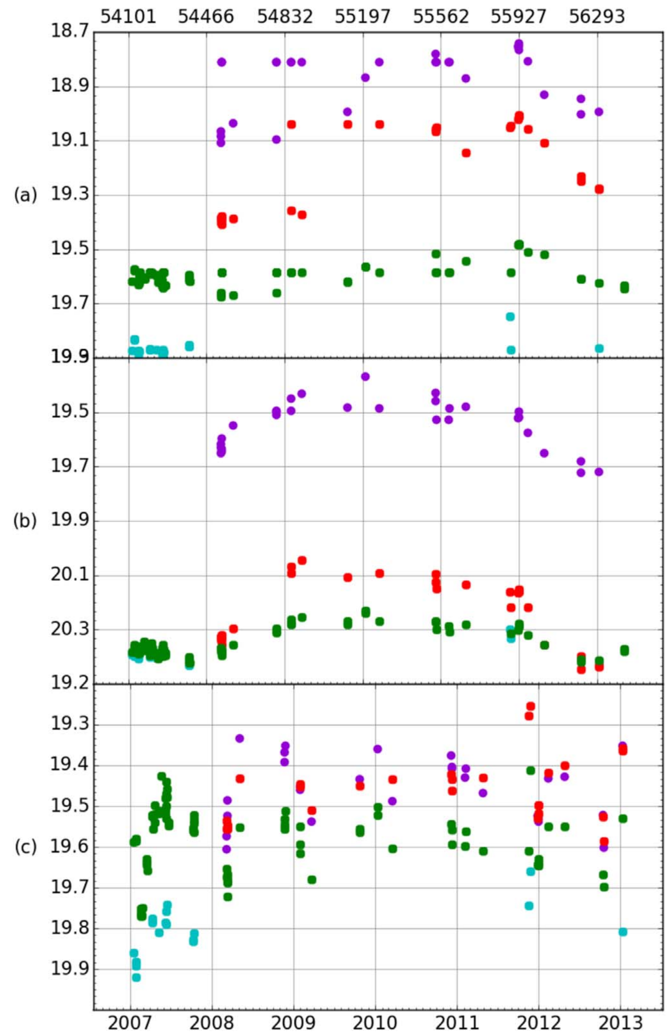

Figure 7. The light curves for (a). I2(ZH 364), (b). I1(ZH 244) and (c). ZH 354. The color code is the same as in Figure 2.

Table 4
Classification Comparison

Star ID	This Paper	Previous Type	Reference[a]	Comments
NGC 2403				
ZH542	F V	H II	3	neb em superposed
ZH553	A8 Ia	A5 Ia	1	IVa28, see the text
ZH583	A:	H II	3	low S/N
ZH 585	F2 I	LBVc[b]	3	
ZH 730	A5	F0	1	N2403-80 (Humphreys & Aaronson 1987b), High Vel, Horiz Br star:
ZH912	A0-2 I	A8 Ia	1	neb em
S29	A0	LBVc	3	broad H abs, neb em, prob foregrd
S44	early F	LBVc	3	low S/N
S94	F5 Ia	LBVc	3	see the text
S185	F8 V	LBVc	3	narrow H abs, Horiz Br star:
V38	LBV	LBVc	3	see the text
V52	F8 V	LBVc	3	see the text
M81				
ZH224	F2-5 I	H II + blue cont.	4	neb em
	…	LBVc	2	
ZH235	H II	H II	2	
ZH364(I2)	LBVc	LBV	2	see the text
ZH372	F5 I	SGc(F)	2	
ZH479	F V	SNRc	2	
ZH491	foreground	SGc(G)	2	v.red, molecular bands?
ZH501	H II	H II	4	strong neb em, He I em
	…	H II	2	
ZH628	G V	G field	4	
	…	FG field	2	
ZH679	A8 I	H II	2	H em
ZH1143	F2 Ia	F2 Ia	1	M81-75, H em, neb em
ZH1406(I8)	F5 I	LBVc	2	see the text
I3	F5 V	LBVc	2	see the text

Notes.
[a] References for previous types: (1) Humphreys & Aaronson (1987b), (2) Sholukhova et al. (1998b), (3) Sholukhova et al. (1998a), (4) Zickgraf et al. (1996).
[b] Candidate LBV.

4. Interstellar Extinction, the Spectral Energy Distributions, and Circumstellar Dust

The lack of a uniform data set for the visual photometry and limited coverage in the near-infrared in N2403 and M81 complicates a comprehensive survey of the spectral energy distributions for most of the confirmed members.

The visual-wavelength photometry comes from three sources: the Zickgraf & Humphreys (1991) photographic survey, the GO fields in the ANGRR and ANGST programs with *HST*/ACS, and the LBT/LBC survey. No one survey includes all of the stars in Tables 2 and 3. The *HST* fields of course have the highest spatial resolution but usually include only two colors, visual and blue. The LBC data set includes *UBVR*[4] magnitudes, but is seeing limited. The formal errors listed for the stars in the LBT/LBC survey are quite small, typically 0.03–0.02 mag and less, and are smaller than the dots on the light curves shown in Figures 2, 5, and 7. The majority of stars in Tables 2 and 4 are in this set.

In addition, we used the DOLPHOT package for WFC3/IR to measure near-infrared VEGA magnitudes at 1.1 and 1.6 microns from GO11719 and GO 13477 for N2403 and from GO12531 and GO11731 for M81. Due to the limited spatial coverage, only eight confirmed members in N2403, and nine in M81 have measured near-infrared magnitudes. We also measured mid-infrared magnitudes from the *Spitzer* IRAC surveys. We used the median mosaic images in all four IRAC bands from the *Spitzer* archive. The MOPEX/APEX package was then used to measure point response fitting photometry with the detection limit set at 3σ. Many of the stars were too faint to be detected, and the photometry is further complicated by the high backgrounds and complex extended regions where they are found. Therefore, each image was inspected individually.

We list all of the available photometry for the confirmed members in Table 5, with the exception that the photographic magnitudes are listed only if no other source is available.

[4] The *UBV* magnitudes are on the Johnson system but *R* is Cousins-Kron.

Table 5
Multi-Wavelength Photometry

Star ID	U[a]	B[a]	V[a]	R[a]	F435[b]	F475[b]	F606[b]	1.1 μm	1.6 μm	3.6 μm (μJy)	4.5 μm (μJy)	5.8 μm (μJy)	8 μm (μJy)	Comments
						NGC 2403								
ZH 585[c]	19.85	19.51	19.43	18.91	…	…	…	…	…	13	1.6	…	…	…
ZH 553	18.24	18.21	…	18.0	…	…	…	…	…	38	12	…	…	…
ZH 335	19.98	19.46	19.19	19.05	…	…	…	…	…	22	9	…	…	…
ZH 2328[c]	…	…	20.04	…	…	…	…	…	…	…	…	…	…	…
ZH 1521	19.09	18.86	18.59	18.43	…	…	19.98	…	…	50	73	…	…	…
ZH 533	18.66	19.24	19.36	19.39	…	…	…	…	…	…	…	…	…	…
ZH 2313[c]	…	…	19.78	…	…	…	…	…	…	111	21	…	…	complex region
ZH 2562[c]	…	…	19.57	…	…	…	…	…	…	130	27	…	…	H II?
ZH 2022[c]	…	…	19.95	…	…	…	…	…	…	…	…	…	…	…
10182-pr-9	…	…	…	…	…	19.60	19.49	…	…	…	…	…	…	…

Notes.
[a] LBT/LBC magnitude unless designated otherwise as a footnote to the star ID or in Comments.
[b] Magnitude from *HST* images, see the text.
[c] Photographic *UBVR* magnitudes from Zickgraf & Humphreys (1991).
[d] $V = 19.31$, $B–V = 0.53$ Sandage (1984b).

(This table is available in its entirety in machine-readable form.)

To determine whether these stars have excess free–free emission from their stellar winds and/or circumstellar dust, as well as their intrinsic luminosities, we must first correct their SEDs for interstellar extinction. For stars with multi-wavelength visual photometry and spectral types, we adopt the Cardelli et al. (1989) extinction curve with $R = 3.2$ and follow the standard procedure and estimate the reddening $E(B–V)$ and visual extinction A_v from their observed colors and spectral types. However, broadband colors cannot be safely used for stars with strong emission lines. In our previous work on M31 and M33, we adopted the mean extinction from nearby stars and from the H I column density. However, extensive catalogs of resolved stars in the fields of N2403 and M81 do not yet exist, and the neutral hydrogen maps have much lower spatial resolution at their larger distances. In our detailed study of V37 and V12 in N2403 (Humphreys et al. 2017b), we determined visual extinctions of 0.54 mag and 0.9 mag, respectively from the stars in their near environments. In this work, we find a mean extinction for the confirmed supergiants of 0.47 mag. We have a similar situation in M81. Kudritzki et al. (2012) found a mean color excess of 0.26 mag or A_v of 0.9 mag from their quantitative analysis of 25 early-type stars in M81. Our mean extinction for the confirmed supergiants in M81 is a very similar 0.86 mag. Therefore, in this study we adopt total visual extinctions (A_v) of 0.5 and 0.9 magnitudes respectively in N2403 and M81, for the emission-line stars, the LBVs and sgB[e]'s, and for those stars which lack complete photometry. In Table 6, we summarize the results for the confirmed stellar members with adopted distance moduli of 27.5 mag for N2403 and 27.8 for M81 from Cepheids (Freedman et al. 2001) to derive their corresponding absolute visual magnitudes.

4.1. The Spectral Energy Distributions (SEDs)

Despite the limitations of the multi-wavelength photometry and especially the lack of infrared data for many of the stars, we show a selected sample of SEDs in Figure 8, specifically of stars of interest such as the LBV candidates, the sgB[e]'s, and and others with possible circumstellar dust.

The SEDs for the two LBV candidates in M81 are shown in the top panel. Since these are strong emission-line stars, their photometry is corrected for interstellar extinction using the mean A_v. ZH 364(I2) has a near-infrared excess that we attribute to free–free emission. Its spectrum shows a strong Hα emission line with broad wings. We also note the raised photometric points in its SED in the R-band due to Hα and in the U-band possibly due to continuum emission. Thus, its near-infrared excess is most likely due to free–free emission and not warm dust. We show Planck curve fits to their corrected broadband data to estimate the temperature shown and integrated to derive a luminosity ($M_{\rm Bol}$) in Table 6. However, the temperature for ZH 354 from the fit to the LBT/LBC photometry is inconsistent with the much higher temperature implied by its emission lines such as He II in its spectrum (Figure 6). It is possible that the extinction correction is much larger than the adopted mean, or the LBC photometry is identified with the wrong star. Its luminosity derived from the SED is not used for this reason.

The SEDs for two sgB[e] stars with infrared data are shown in the middle panel. Their mid-infrared fluxes demonstrate the presence of significant circumstellar dust as found for many sgB[e]'s in other galaxies (Kraus et al. 2014; Humphreys et al. 2017c). Although the optical photometry for 10584-8.4 in M81 is limited, its SED exhibits a large circumstellar excess due to dust plus extensive circumstellar gas revealed by the [Ca II] and Ca II emission lines in its red spectrum, Section 3.1. The mid-infrared fluxes may seem high or elevated with respect to the visual photometry; however, this strong infrared signature for circumstellar dust is not uncommon for sgB[e]'s (Humphreys et al. 2017a, 2017c). Although the absorption lines in its blue spectrum suggest a late B/early A classification, the Planck fit to the nonuniform optical photometry yields a temperature of 21700 K. We

Table 6
Interstellar Extinction and Luminosities (in magnitudes)

Star ID	Sp Type	$B - V$ (LBC)	$B - V$ (*HST*)	E_{BV}	A_V	M_V	$M_{\rm Bol}$	Temp.[a]
			NGC 2403					
ZH 585	F2 I	0.08	⋯	⋯	0.5	−8.6	−8.5	7000
ZH 553	A8 I	⋯	⋯	⋯	0.5	−9.6:	−9.5:	8200
ZH 335	F0 I	0.27	⋯	0.07	0.22	−8.5	−8.4	7800
ZH 1521	F2 I	0.27	⋯	0.01:	0.5	[b]	−8.0	7400
ZH 533	B5: I	−0.12	⋯	0.05:	0.5	−8.68	−9.5	13700
ZH 2313	A0-A2	⋯	⋯	⋯	0.5	−8.26	−8.5	9500
ZH 2562	B I	⋯	⋯	⋯	0.5	−8.47	−10:	20000:
ZH 2022	B8 I	⋯	⋯	⋯	0.5	−8.09	−8.6	10900
10182-pr-9	WN	⋯	0.11	⋯	⋯	⋯	⋯	⋯
ZH 2016	WN	⋯	⋯	⋯	⋯	⋯	⋯	⋯
10182-pr-1	A5-A8 I	⋯	0.36	0.24	0.77	−9.17	−9.1	8300
ZH 946	B5 I:	0.05	⋯	0.0:	0.5	−8.3	−9.3	13700
ZH 947	B5 I	−0.21	⋯	⋯	0.5	−8.98	−10.0	13700
10182-pr-2[c]	F5 I	1.33	1.28	1.00	3.2	−11.7:	−11.6	7000
10182-pr-6	A8-F0 I	0.89	1.00	0.7–0.8	2.4	−10.4:	−10.3	8000
10182-pr-15	A0-A2 I	0.17	0.35	0.12–0.30	0.96	−8.6	−8.8	9500
10182-pr-16	B8 I:	−0.14	0.08	0.05	0.16	−7.7	−8.2	10900
ZH 729	B8 I	0.15	⋯	0.20	0.64	−8.9	−9.4	10900
ZH 2248	A0 I	⋯	⋯	⋯	0.5	−8.3	−8.6	9800
V38	LBV	−0.02	⋯	⋯	0.5	−8.6	−10.25	(18950)
ZH 931	A5-A8 I	0.27	⋯	0.15	0.48	−8.0	−8.1	8300
ZH 1938	A2 I	⋯	⋯	⋯	0.5	−8.7	−8.9	9100
S94	F5 I	0.53	⋯	0.20	0.64	−8.8	−8.8	7000
ZH 924	B5-B8 I	−0.13	⋯	0.0:	0.5	−8.7	−9.4	12000
ZH 912	A0-A2 I	0.2	⋯	0.15	0.48	−9.6	−9.8	9500
ZH 884	F0 I	0.07	⋯	⋯	0.5	−9.3	−9.3	7800
			M81					
10584-11-1	A5 I	0.27	0.35	0.25	0.8	−9.1	−9.1	8500
ZH 679	A8 I	0.27	⋯	0.13	0.42	−8.5	−8.4	8200
10584-8-4	sgB[e]	⋯	0.25	⋯	(0.9)	⋯	−9.4	(21700)
10584-4-1	sgB[e]	0.04	0.36	⋯	(0.9)	⋯	−10.7	(19671)
ZH 372(10584-15-1)	F5 I	0.38	0.50	0.17	0.54	−8.8	−8.7	7000
10584-8-1	F0 I	0.45	0.53	0.25–0.33	0.8–1.06	−9.5	−9.4	7800
10584-8-2	F0 I	0.41	0.49	0.21–0.29	0.7–0.9	−9.1	−9.0	7800
ZH 244(I1)(10584-19-1)	A I	0.04	1.29:	0 -?	(0.9)	−9.1	−9.1	9000:
10584-9-1	sgB[e]	0.24	0.35	⋯	(0.9)	⋯	−11.0	(18000)
ZH 364(I2)(10584-16-1)	LBVc	0.27	1.54	⋯	(0.9)	⋯	−10.4	(15860)
10584-5-2	F5 I	0.23	0.38	0.05	0.16	−7.9	−7.8	6200
ZH 224 (10584-23-1)	F2-5 I	0.47	1.58:	0.22	0.70	−9.7	−9.6	7200
10584-13-2	F2 I	0.69	0.69	0.43	1.38	−9.4	−9.3	7400
10584-10-5	A I + WN	0.10	0.38	⋯	⋯	⋯	⋯	⋯
10584-20-2	B5 I	0.86:	0.20	0.28	0.90	−9.2:	−10.0	13700
10584-13-3	F8 I	1.36	1.27	0.8	2.56	−10.3:	−10.2	6200
ZH 354	LBVc	0.1	⋯	⋯	(0.9)	⋯	⋯	⋯
10584-14-2	G0 I	0.78	0.81	0.20	0.64	−8.7	−8.7	5500
ZH 1143 (10584-24-1)	F2 I	0.42	1.42:	0.16	0.51	−9.55	−9.45	7400
ZH 1406(I8)(10584-18-1)	F5 I	0.51	0.61	0.23	0.74	−9.2	−9.1	7000
10584-25-2	G0 I	1.0	1.0	0.35	1.12	−9.7	−9.7	5500
10584-18-5	A8 I	0.16	0.27	0.13	0.41	−8.3	−8.2	8200

Notes.
[a] Temperatures based on the Planck fit to the SED are in parentheses.
[b] M_v depends on the adopted visual magnitude: −9.45(LBC), −8.06(*HST*).
[c] Note exceptionally high luminosity. Its *HST* image in Figure B1 shows it is extended.

consider this result doubtful, though, because the fit is dominated by the uncertain U band point from the LBT/LBC imaging. Using only the *HST* magnitudes, the best fit yields 10900 K. 10584-9.1 is a much hotter star as indicated both by is spectrum and SED. The Planck fit to the optical photometry suggests a temperature of 18000 K. Its mid-infrared excess may be a combination of free–free emission and dust.

We also show the SEDs for two luminous intermediate-type supergiants in the bottom panel. 10584-8.1 may have circumstellar dust, although its spectrum did not show any

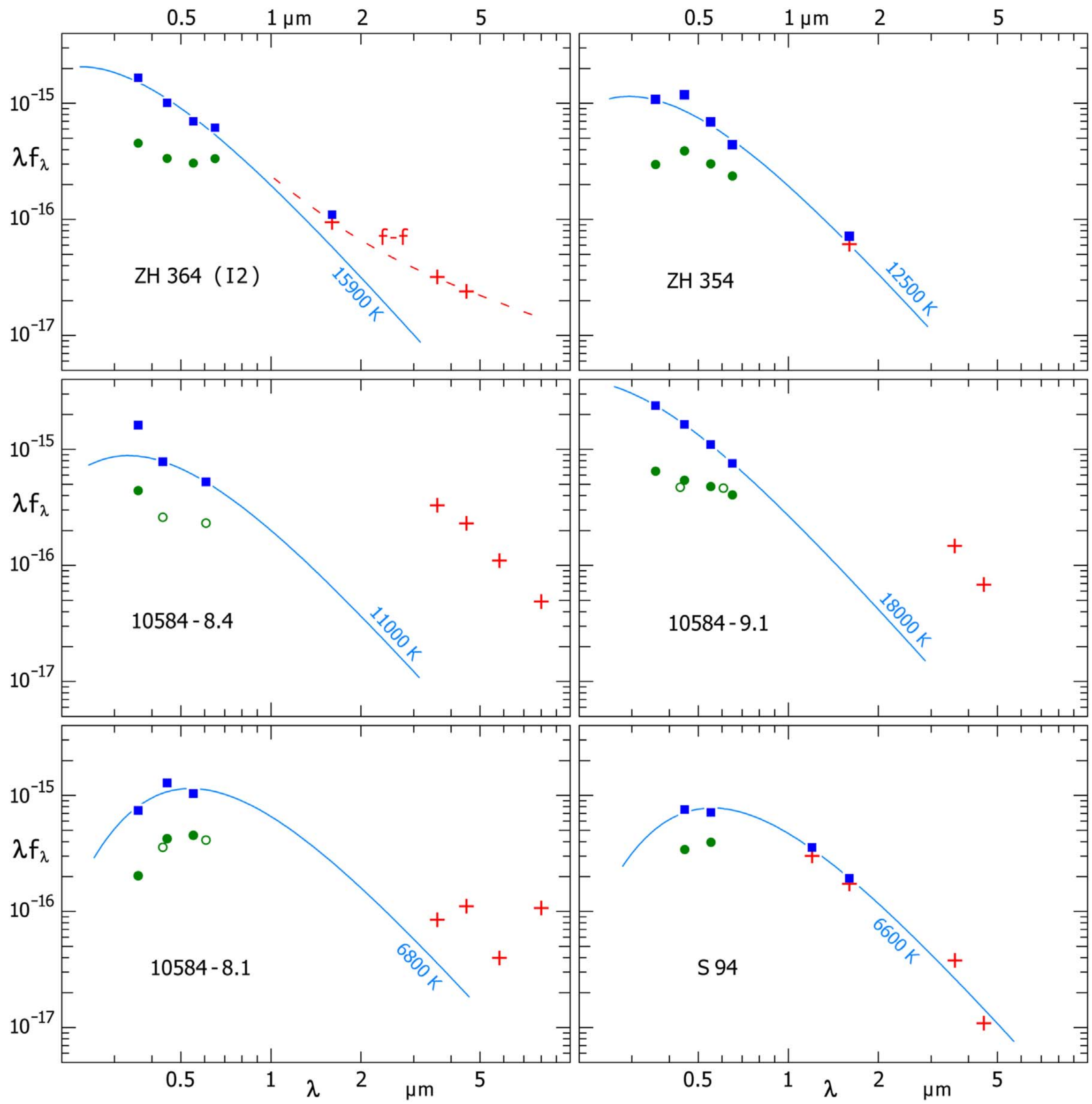

Figure 8. The SEDs for six luminous stars to illustrate the presence or lack of circumstellar dust. The green dots are the observed LBT/LBC visual-wavelength magnitudes and the blue boxes show the same photometry corrected for interstellar extinction (Table 6). The open circles show the magnitudes from the *HST*/ACS images when available. The red crosses are the near-IR magnitudes from the *HST*/WFC3 images and from Spitzer/IRAC. The statistical 1σ errors are smaller than the dots in these log–log plots.

stellar wind emission lines. Planck curve fits to their optical photometry are shown.

The temperatures and derived luminosities estimated in this way are used to place the emission-line stars on the HR Diagram discussed in the next section. We note, as per usual, that Planck curves are only rudimentary approximations.

5. The HR Diagrams

The HR Diagrams for the confirmed stellar members in NGC 2403 and M81 from Table 6 are shown in Figures 9 and 10, respectively. The bolometric luminosities and temperatures in Table 6 are adopted from the calibrations by Flower (1996) for the supergiants, from Martins et al. (2005) for the O-type stars, and from the Planck fits to the SEDs for the emission-line stars. We added the late B- and early A-type supergiants in M81 from Kudritzki et al. (2012). The temperatures are derived from the data in their Table 3, and their derived luminosities are corrected to our adopted distance modulus.[5]

The uncertainty in the placement of the individual stars on the HR Diagrams will vary from star to star. A major source is the adopted *B*–*V* colors and the interstellar extinction. The range in the observed *B*–*V* colors (Table 6) is $\approx\pm0.1$ mag, which will translate to an uncertainty up to 0.3 mag in M_V. For example, two stars, 10182-pr-6 in NGC 2403 and 10584-13-3 in M81, lie just to right of the upper luminosity boundary or Humphreys–Davidson limit shown in Figure 11. While this could be real and indicative of their evolved state, both stars have notably high values of total interstellar extinction (A_V), and as was noted in Table 2, 10182-pr-6 may be more than one star based on its spectral features.

[5] Kudritzki et al. (2012) derived a distance modulus of 27.7 mag for M81, while we have adopted 27.8 mag based on Cepheids (a small difference).

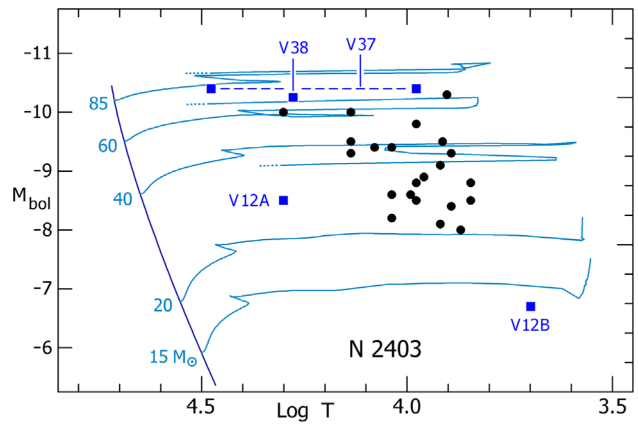

Figure 9. The HR Diagram for NGC 2403 stars presented in this paper. The positions of the confirmed LBVs V37 and V38 are identified. V37's position is shown during its high mass-loss state in 2002 and in quiescence. The surviving star from V12's (SN 1954J) giant eruption and its less luminous cooler companion are plotted as V12A and V12B. The evolutionary tracks with mass loss are from Ekstrom et al. (2012) without rotation.

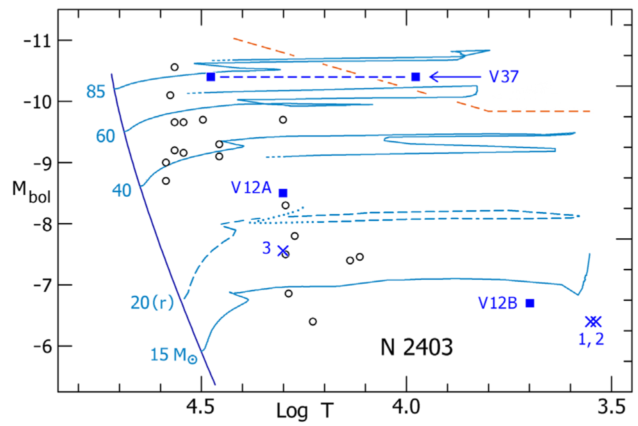

Figure 11. An HR Diagram illustrating the stellar population and nearby stars in the near environments of V37, plotted as open circles, and for the giant eruption V12. Its neighbors within ∼1 arcsec, stars 1, 2, and 3, are shown as blue crosses. V12 itself is not resolved in the *HST* images but its spectrum shows it is two stars; the hot star V12A, the likely survivor, has a cooler less luminous neighbor V12B. In this HRD, we show the 20 $M_{\odot}$ track with mass loss and rotation (Ekstrom et al. 2012) to illustrate the likely post-red supergiant evolutionary state for V12A. The dashed red line is the upper luminosity boundary (Humphreys & Davidson 1979, 1994).

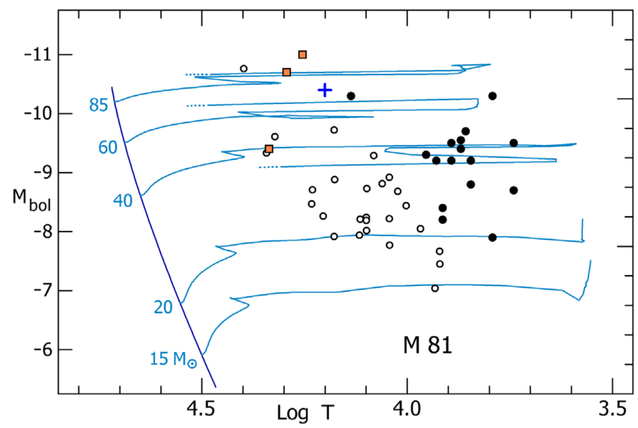

Figure 10. The HR Diagram for M81. The stars presented this paper are plotted as filled circles and those from Kudritzki et al. (2012) as open circles. The position of the candidate LBV I2 (ZH 364) is shown as a blue cross and the three B[e] supergiants as orange squares. The LBV candidate ZH354 is not shown. Its available photometry is not consistent with its spectrum.

The LBV V37 (SN 2002kg) and the giant eruption/SN impostor V12 (SN 1954J) both in NGC 2403 are the only two stars in our survey with available data for their neighboring stars (Van Dyk et al. 2006; Humphreys et al. 2017b). For that reason, we show a separate HRD in Figure 11 for these two stars and their stellar environments. We used the two-color diagram for the stars near V37 (Van Dyk et al. 2006) plus the Q-method to estimate their intrinsic *B–V* colors, corresponding spectral types, and interstellar extinction from which we derived their visual and absolute bolometric magnitudes to place them on the HRD shown here.

V37 is associated with other reddened hot stars and is one of the most massive in its environment. It is not known if V12 is a physical pair but its companion is a G-type supergiant, and its nearby neighbors include a hot supergiant and two red supergiants. Thus, both are closely associated with other evolved stars. Neither is isolated, as has been suggested for some LBVs (Smith & Tombleson 2015). Based on its temperature and luminosity, V12(A) will lie just below the LBV instability strip on the HR Diagram (Humphreys et al. 2016). Like the "less luminous" LBVs, V12 was very likely a post-red supergiant, and having shed a lot of mass, it was close to its Eddington limit at the time of its giant eruption. In Figure 11, we show the evolutionary track for a 20 $M_{\odot}$ star with mass loss and rotation (Ekstrom et al. 2012) that illustrates probable post-RSG evolution. Note the short transit back to cooler temperatures at the end of the track near the likely position of V12A's progenitor, an ideal state for a highly evolved star to experience an eruption.

Research by R.H. on massive stars was supported by the National Science Foundation grant AST-1109394. We thank Schuyler Van Dyk for sharing the optical photometry for the stars in the near environment of V37(SN 2002kg) used for his Figure 9 in Van Dyk et al. (2006).

Facilities: MMT/Hectospec, LBT/LBC, *HST*/ACS, *HST*/WFC3.

Appendix A
Foreground Stars

This Appendix section comprises a table (Table 7) of foreground stars and other objects.

Table 7
Foreground Stars and Others

Star ID	Position *J*2000	Sp. Type	*V*	Source	Variability	Comments
NGC 2403						
ZH 2141 (F2)	7:35:13.38 65:37:2.01	A2	201.13	1	⋯	Horiz. br star:
ZH 601 (F1+F2)	7:35:22.74 65:37:26.30	F5 V	19.66	1	⋯	⋯
ZH 1882 (F1+F2)	7:35:22.83 65:35:21.09	⋯	19.97	1	⋯	low S/N
ZH 608 (F2)	7:35:22.94 65:39:9.78	F5 V	18.41	1	⋯	
ZH 604 (F1)	7:35:29.94 65:39:20.71	pec	19.56	1	var:	pec em, low S/N
ZH 803 (F2)	7:35:36.57 65:39:20.57	A5	201.19	1	⋯	low S/N
ZH 360 (F1+F2)	7:35:37.63 65:33:50.97	⋯	20.05	1	⋯	low S/N
ZH 583 (F2)	7:35:41.00 65:35:59.15	A:	19.91	1	⋯	low S/N
ZH 2125 (F1)	7:35:42.92 65:37:44.33	⋯	19.5	1	⋯	low S/N, foreground
ZH 593 (F2)	7:35:43.26 65:38:21.20	A:	20.12	1	⋯	low S/N, foreground
ZH 2131 (F1)	7:35:43.51 65:38:39.81	⋯	19.31	1	⋯	low S/N
ZH 790 (F1+F2)	7:35:53.66 65:39:35.24	A8	19.77	1	⋯	⋯
ZH 569 (F1)	7:35:53.76 65:34:53.01	⋯	20.08	1	⋯	neb em superposed
ZH 190 (F1+F2)	7:35:58.27 65:29:43.74	A2	19.35	1	⋯	Horiz. br. star:
ZH 1005 (F1+F2)	7:35:58.86 65:44:55.60	A5	18.31	1	var:	Horiz. br. star:
ZH 1001 (F1+F2)	7:35:59.71 65:43:01.14	F5 V	17.97	1	⋯	High vel star
ZH 566 (F2)	7:36:00.91 65:35:16.73	⋯	19.86	1	⋯	v low S/N, pec
ZH 565 (F1+F2)	7:36:04.24 65:35:48.09	⋯	19.56	1	var:	pec:, low S/N
ZH 991 (F2)	7:36:07.44 65:41:55.23	F5 V	19.58	1	⋯	
ZH 1819 (F1+F2)	7:36:20.17 65:28:42.21	F5 V	17.97	1	⋯	⋯
ZH 552 (F2)	7:36:24.26 65:35:51.06	A5	19.64	1	⋯	neb em, H em superposed
ZH 542 (F1+F2)	7:36:27.42 65:33:49.64	F V	20.07	1	⋯	neb em superposed
ZH 1100 (F1+F2)	7:36:32.43 65:43:56.36	⋯	20.2	1	⋯	low S/N, foreground
S44 (F2)	7:36:38.96 65:35:32.27	early F	19.59	5	⋯	low S/N
ZH 1097 (F1+F2)	7:36:42.74 65:44:9.38	F8 V	18.73	1	⋯	⋯
ZH 732 (F2)	7:36:45.02 65:38:50.60	F5 V	20.05	1	⋯	neb em
10182-p2-22 (F2)	7:36:49.63 65:36:22.57	G: V	20.08	2	⋯	H em superposed
10579-x1-2 (F2)	7:36:49.79 65:35:49.69	G: V:	19.58	3	⋯	neb em, H em superposed
V52 (F1)	7:36:50.39 65:37:52.1	F8 V	20.10	4	⋯	
S29 (F2)	7:36:52.35 65:34:53.58	early A	18.89	5	⋯	br H abs, neb em superposed
ZH 2276 (F2)	7:36:56.99 65:38:1.57	F0 V	19.68	1	⋯	neb em
ZH 730 (F1)	7:37:00.29 65:37:55.25	A5	18.16	1	⋯	High vel star, Hor.Br?, N2403-80 (Humphreys & Aaronson 1987b)
S185 (F2)	7:37:02.42 65:35:54.64	F8 V	17.84	5	⋯	narrow H abs., Horiz Br?
ZH 1081 (F1)	7:37:08.38 65:42:13.64	⋯	18.98	1	⋯	low S/N, pec
ZH 292 (F1+F2)	7:37:11.31 65:28:32.69	G0 V	18.74	1	⋯	⋯
ZH 932 (F2)	7:37:13.49 65:40:18.07	A:	19.91	1	⋯	low S/N
ZH 923 (F2)	7:37:21.05 65:39:11.48	A8	18.1	1	⋯	Horiz Br?
ZH 1079 (F1+F2)	7:37:21.35 65:42:47.77	⋯	18.68	1	⋯	low S/N
ZH 480 (F2)	7:37:21.62 65:32:32.53	A5	19.75	1	⋯	⋯
ZH 2600 (F1+F2)	7:37:24.04 65:40:46.79	F2-F5 V	19.49	1	⋯	⋯
ZH 1064 (F1+F2)	7:37:48.52 65:40:53.14	F5-F8 V	18.8	1	⋯	⋯
ZH 897 (F1)	7:37:50.46 65:38:35.70	late A	19.32	1	⋯	low S/N
ZH 1061 (F2)	7:37:56.58 65:39:15.43	foreground	18.94	1	⋯	red only
ZH 2455 (F1+F2)	7:37:59.50 65:37:25.69	F2 V	19.58	1	⋯	⋯
ZH 418 (F1+F2)	7:38:9.62 65:26:44.31	⋯	19.51	1	⋯	low S/N
ZH 869 (F1+F2)	7:38:23.77 65:36:38.69	QSO	19.74	1	var	⋯
M81						
ZH 400	9:54:18.65 69:02:45.65	galaxy	19.43	1	⋯	redshifted
ZH 512	9:54:20.69 69:09:13.09	⋯	19.62	1	⋯	poor S/N
10584-3.1	9:54:27.43 69:08:59.07	⋯	19.97	6	⋯	low S/N
ZH 1355	9:54:34.94 69:01:54.92	F: V	19.75	1	⋯	neb em, low S/N

Table 7
(Continued)

Star ID	Position J2000	Sp. Type	V	Source	Variability	Comments
ZH 833	9:54:50.64 69:14:44.83	F5 V	19.85	1	⋯	Horiz Br?
ZH 491	9:54:56.81 69:4:55.16	⋯	19.63	1	⋯	v.red, molecular bands
ZH 1389	9:55:00.11 69:06:14.05	F V	19.88	1	⋯	neb em
ZH 904	9:55:03.60 69:16:43.73	A5	19.72	1	⋯	Horiz Br
ZH 1209	9:55:15.78 69:5:47.14	F2 V	19.14	1	⋯	⋯
ZH 228	9:55:42.39 68:58:22.39	F: V	19.99	1	⋯	low S/N
ZH 108	9:55:44.55 68:51:52.70	neb em	20.09	1	⋯	red sp. only
ZH 619	9:55:51.71 69:04:40.96	F8 V	20.03	1	⋯	⋯
ZH 628	9:55:51.90 69:07:39.05	G V	18.66	1	⋯	⋯
10584-10.4	9:55:51.98 69:12:9.57	F8 V	19.41	6	⋯	Horiz Br star
10584-21.4	9:55:55.03 69:00:56.28	F5 V	19.61	6	⋯	⋯
10584-10.1	9:56:2.63 69:11:45.27	G V	19.44	6	⋯	⋯
ZH 623	9:56:03.22 69:08:09.43	F5 V	18.48	1	⋯	Horiz Br?
I3	9:56:08.50 69:03:51.24	F5 V	19.6	7	⋯	LBV cand., see the text
10584-10.2	9:56:11.26 69:10:47.26	F V	19.51	6	⋯	⋯
ZH 479	9:56:20.54 69:2:48.46	F V	19.14	1	⋯	⋯
10584-21.8	9:56:24.16 69:00:29.28	F V	19.91	6	⋯	⋯
10584-21.2	9:56:27.52 69:01:10.04	F5 V	19.52	6	⋯	Horiz Br
10584-21.5	9:56:27.55 69:01:9.95	F V	19.65	6	⋯	red sp. only
ZH 642	9:56:33.06 69:08:02.69	⋯	19.1	1	⋯	poor S/N
ZH 344	9:56:33.07 68:58:30.15	A	19.24	1	⋯	Horiz Br
ZH 92	9:56:35.17 68:50:45.28	A-F V	19.94	1	⋯	⋯
10584-22.3	9:56:36.47 69:00:28.78	QSO	20.69	6	⋯	⋯
10584-22.1	9:56:49.54 69:03:13.11	A-type WD	19.8	6	⋯	⋯
ZH 865	9:56:53.05 69:10:27.22	G V	19.59	1	⋯	⋯
ZH 454	9:56:58.29 69:00:45.92	pec em QSO?	19.93	1	⋯	⋯
ZH 324	9:57:01.56 68:55:0.29	QSO:	17.87	1	⋯	pec em

Note.
[a] Primary Sources for targets: (1) Zickgraf & Humphreys (1991), (2) GO-10182(PI), (3) GO-10579(PI), (4) Tammann & Sandage (1968), (5) Sandage (1984a), (6) GO-10584(PI), (7) Sandage (1984b).

Appendix B
Snap-shot Images

Snap-shot images of 12 of the confirmed members in NGC 2403 and 18 in M81 with images on the *HST/HLA/ACS* frames. Each image is 10″ on a side and the star is marked.

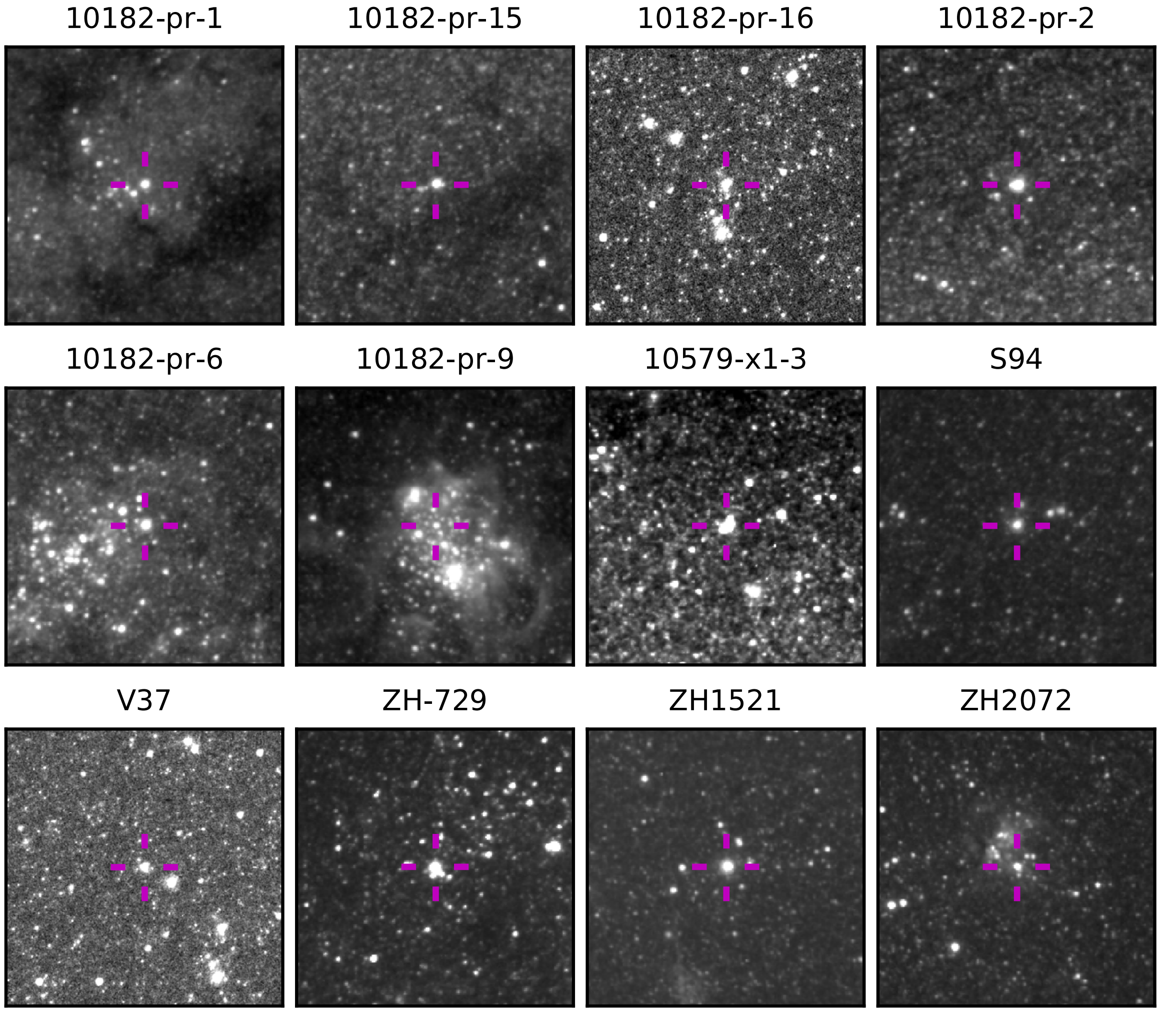

Figure 12. Images of 9 confirmed members in NGC2403 from ACS frames.

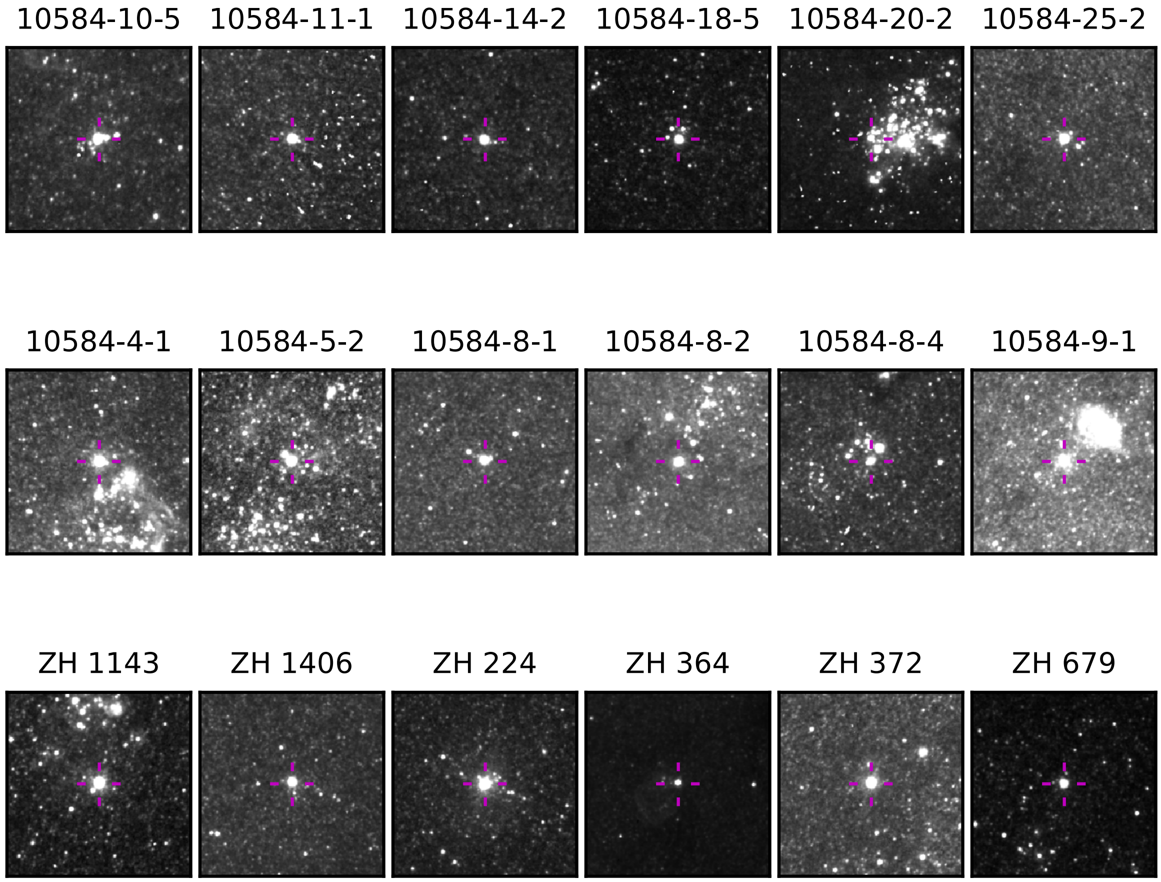

Figure 13. Images of 18 confirmed members in M81 from ACS frames.

ORCID iDs

Roberta M. Humphreys https://orcid.org/0000-0003-1720-9807
Michael S. Gordon https://orcid.org/0000-0002-1913-2682

References

Aret, A., Kraus, M., & Slecha, M. 2016, MNRAS, 456, 1424
Cardelli, J. A., Clayton, G. C., & Mathis, J. S. 1989, ApJ, 345, 245
Ekstrom, S., et al. 2012, A&A, 537, A146
Fabricant, D., Fata, R., Roll, J., et al. 2005, PASP, 117, 1411
Fabricant, D. G., Hertz, E. N., Szentgyorgyi, A. H., et al. 1998, Proc. SPIE, 3355, 285
Flower, P. J. 1996, ApJ, 469, 355
Freedman, W. L., Madore, B. F., Gibson, B. K., et al. 2001, ApJ, 553, 47
Gerke, J. R., Kochanek, C. S., & Stanek, K. Z. 2014, MNRAS, 450, 3289
Gordon, M. S., Humphreys, R. M., & Jones, T. J. 2016, ApJ, 825, 50
Grammer, S. H., Humphreys, R. M., & Gerke, J. 2015, AJ, 149, 152
Humphreys, R. M. 1980, ApJ, 241, 598
Humphreys, R. M., & Aaronson, M. 1987a, ApJL, 381L, 69
Humphreys, R. M., & Aaronson, M. 1987b, AJ, 94, 1156
Humphreys, R. M., Aaronson, M., Lebofsky, M., et al. 1986, AJ, 91, 808
Humphreys, R. M., & Davidson, K. 1979, ApJ, 232, 409
Humphreys, R. M., & Davidson, K. 1994, PASP, 106, 1025
Humphreys, R. M., Davidson, K., & Grammer, S. H. 2013, ApJ, 773, 46
Humphreys, R. M., Davidson, K., Hahn, D., Martin, J. C., & Weis, K. 2017a, ApJ, 844, 40
Humphreys, R. M., Davidson, K., Van Dyk, S. D., & Gordon, M. S. 2017b, ApJ, 848, 86
Humphreys, R. M., Gordon, M. S., Martin, J. C., Weis, K., & Hahn, D. 2017c, ApJ, 836, 64
Humphreys, R. M., Weis, K., Davidson, K., & Gordon, M. S. 2016, ApJ, 825, 64
Kochanek, C. S., Beacom, J. F., Kistler, M. D., et al. 2008, ApJ, 684, 1336
Kraus, M., Cidale, L. S., Arias, M. L., Oksala, M. E., & Borges Fernandes, M. 2014, ApJL, 780, L10
Kudritzki, R.-P., Urbaneja, M. A., Gazak, Z., et al. 2012, ApJ, 747, 15
Martins, F., Schaerer, D., & Hillier, D. J. 2005, A&A, 436, 1049
Sandage, A. 1984a, ApJ, 89, 621
Sandage, A. 1984b, ApJ, 89, 630
Sholukhova, O. N., Fabrika, S. N., & Vlasyuk, V. V. 1998a, PAZh, 24, 699
Sholukhova, O. N., Fabrika, S. N., Vlasyuk, V. V., & Dodonuv, S. N. 1998b, PAZh, 24, 591
Smith, N., & Tombleson, R. 2015, MNRAS, 447, 598
Tammann, G. A., & Sandage, A. 1968, ApJ, 151, 825
Van Dyk, S. D., Li, W., Filippenko, A. V., et al. 2006, arXiv:astro-ph/0603025v1
Zickgraf, F.-J., & Humphreys, R. M. 1991, AJ, 102, 113
Zickgraf, F.-J., Szeifert, Th., & Humphreys, R. M. 1996, A&A, 312, 419